

Atomic, electronic, and ferroelectric properties of manganite $RMnO_3$ ($R=Ho, Er, Tm, Lu$) in hexagonal and orthorhombic phases

Chung-Yuan Ren*

Department of Physics, National Kaohsiung Normal University, Kaohsiung 824, Taiwan

(Received 24 November 2008; revised manuscript received 23 January 2009; published 23 March 2009)

Using first-principles calculations, we perform a systematic study of the energetic, atomic, electronic, and ferroelectric properties of the late rare-earth manganites $RMnO_3$ ($R=Ho, Er, Tm, Lu$) in both hexagonal and orthorhombic structures. The hexagonal phase is confirmed to be energetically preferred over the orthorhombic phase. The calculations show that the size of the band gap of the hexagonal manganites is improved when the triangularly frustrated Mn magnetic moments are properly treated. As R approaches the end of the rare-earth series, the polarization in the hexagonal phase increases whereas that in the orthorhombic phase remains practically unchanged. We conclude that the driving force of ferroelectricity in the hexagonal phase is the asymmetric movement of R ions from the centrosymmetric structure. On the other hand, the underlying E -type ordering is the origin of the ferroelectricity observed in the orthorhombic phase. The interplay among the ferroelectricity, magnetic ordering, and lattice structure for the two phases is also discussed in detail.

DOI: 10.1103/PhysRevB.79.125113

PACS number(s): 77.80.-e, 71.15.Mb, 75.80.+q

I. INTRODUCTION

Rare-earth manganites $RMnO_3$ prepared under ordinary synthetic conditions crystallize in the orthorhombic perovskite structure (o - $RMnO_3$) for $R=La$ -Dy with large ionic radius (r_{ion}) and in the hexagonal structure (h - $RMnO_3$) for $R=Ho$ -Lu with smaller r_{ion} . o - $RMnO_3$ manganites show a rich variety of subtle interplay among charge, spin, orbital, and lattice degrees of freedom, for example, colossal magnetoresistance and charge ordering in hole-doped $LaMnO_3$ (Ref. 1) and the recent discovery of multiferroicity in $TbMnO_3$ and $DbMnO_3$.^{2,3} For h - $RMnO_3$, the localized Mn $3d^4$ configuration in MnO_5 bipyramids and the size effect of R ions are responsible for stabilizing the hexagonal structure.⁴ However, by means of special soft-chemistry synthesis,⁵⁻⁷ applying pressure,^{4,8,9} or even epitaxial thin-film growth,^{10,11} the hexagonal structure can be converted into the more dense, albeit metastable orthorhombic phase. In recent years, these late- R multiferroic compounds in both structural phases have attracted increasing attention because of the unusual coexistence of ferroelectric and magnetic orders, with potential applications in controlling electric polarization by external magnetic fields.¹²

In the hexagonal structure, $YMnO_3$ is the prototype of the h - $RMnO_3$ family. The manganites consist of closely packed layers of MnO_5 bipyramids with shared corners in the basal plane. A cooperative tilting of the bipyramids below the Curie temperature T_C displaces R ions along the c axis to render the compounds ferroelectric.¹³ They also show an antiferromagnetic (AFM) order with the Mn moments aligned in a noncollinear (NC) 120° structure within each basal plane.¹⁴⁻¹⁷ However, the Néel temperature T_N is rather low, probably due to the geometrical frustration.¹⁶ Since $T_N \ll T_C$ ($T_C > 600$ K, $T_N \sim 90$ K),¹⁸ the coupling between ferroelectricity and magnetism is expected to be indirect and weak.¹⁹

Notably, a special AFM phase has been observed in o - $HoMnO_3$ with a commensurate “up-up-down-down” ordering in the MnO_2 plane⁷ or the E -type in the Wollan-Koehler standard notation. This magnetic configuration can

also be characterized by the zigzag chains of ferromagnetic (FM) spins, antiferromagnetically coupled to neighboring chains. It is somewhat surprising that the E -type phase was predicted to be stable over a wide region of the phase space.^{20,21} Moreover, both theoretical^{22,23} and experimental^{9,24} works demonstrate the existence of spontaneous polarization triggered by such a magnetic configuration with broken spatial inversion symmetry.

The most significant effect on the orthorhombic structure by decreasing r_{ion} is to enhance the cooperative rotation of the MnO_6 octahedra. The resulting substantial bending of the Mn-O-Mn angle will weaken the FM superexchange interactions between nearest-neighbor Mn ions due to a reduction in the transfer intensity of e_g electrons. Therefore, the AFM interactions between Mn ions from different zigzag chains through the Mn-O-O-Mn (Refs. 8 and 25) or the Mn-O-Mn path^{4,26,27} would need to be taken into account. Competition between these components may be the origin of the magnetic transition from the A type for the large r_{ion} to the E type for the smaller one.

The crystal structure of h - $RMnO_3$ has one major difference when compared to the orthorhombic phase: the Mn ion is located at the center of a trigonal bipyramid instead of an octahedron (Fig. 1). The corresponding crystal field splits the $3d$ orbitals into two doublets $e_{1g}(yz/zx)$ and $e_{2g}(xy/x^2-y^2)$ and one singlet $a_{1g}(3z^2-r^2)$ rather than one triplet $t_{2g}(xy/yz/xz)$ and one doublet $e_g(3x^2-y^2/y^2-z^2)$ under the octahedral environment (Fig. 2). Consequently, the Mn $3d^4$ configuration has no partially filled degenerate level and is less Jahn-Teller (JT) active. Another difference is that the MnO_5 bipyramids in the hexagonal phase are linked in sheets, contrary to the three-dimensional (3D) network of MnO_6 octahedra in perovskite manganites. The cooperative rotations in the orthorhombic phase will force the octahedra around two perpendicular axes to rotate in opposite directions and keep the global inversion symmetry retained,¹³ regardless of the magnetic effect. In h - $RMnO_3$, however, due to the layered structure and the triangular symmetry, the rotations break the inversion symmetry and establish ferroelectricity.

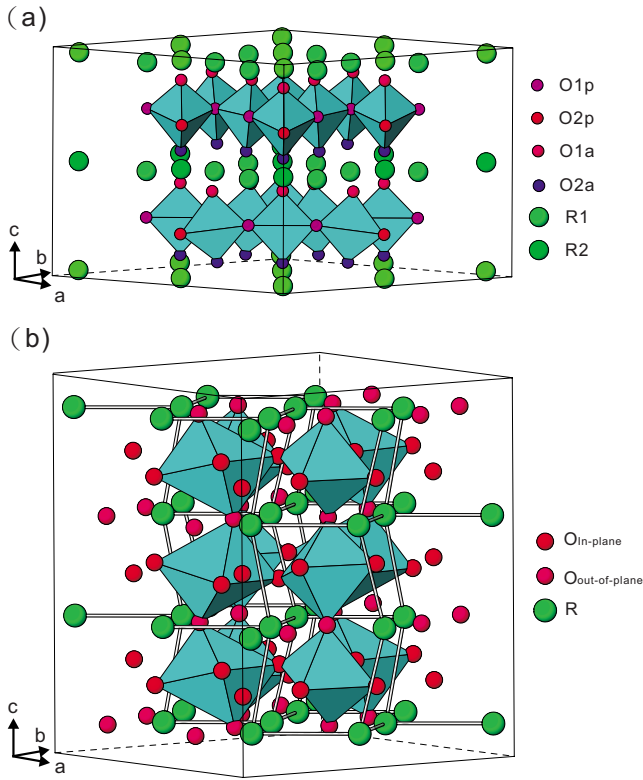


FIG. 1. (Color online) Crystal structure of (a) hexagonal and (b) orthorhombic $RMnO_3$. The large ball represents R ion and the small ball is O anion.

Model studies of multiferroic materials have provided two basic pictures to concern the microscopic origin of electric polarization. One of them is the spin-current model,^{28,29} which predicts that the polarization can be induced by a polar charge distribution even if the ions are not displaced from their centrosymmetric positions. The other is the “lattice mechanism,” which involves magnetically induced ionic displacements and is usually discussed in terms of Dzyaloshinskii-Moriya interactions.^{30,31} However, experiments are generally not sensitive enough to resolve the tiny atomic displacement to distinguish the contributions from the models. First-principles calculations appear to be another appealing alternative to address this issue since the electronic structure and lattice distortion can be treated separately. Furthermore, such a method^{32,33} reveals that both models based on only nearest-neighbor spin interactions are inadequate to describe the polarization in the spiral-spin structure.

Density-functional theory has been used to give an instructive description of h - $YMnO_3$ and o - $HoMnO_3$.^{13,23,34–38} The purpose of this work is devoted to a systematically comparative analysis of the atomic, electronic, and ferroelectric properties of the late- R manganites ($R=Ho, Er, Tm, \text{ and } Lu$) in the two structural phases using first-principles calculations. We aim to study the interplay among the lattice, magnetism, and ferroelectricity. In addition to the energetic preference for the hexagonal phase, it was found that the total-energy difference between the two phases increases as r_{ion} decreases, reflecting the growing difficulty in converting h - $RMnO_3$ to the orthorhombic phase. The size of the band gap for the hexagonal phase agrees better with experiments

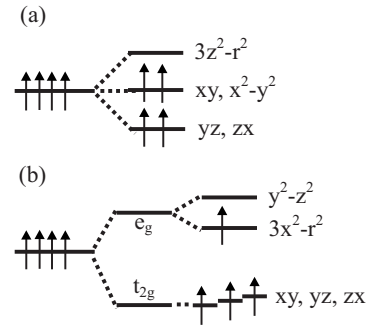


FIG. 2. Schematic illustration of the splitting of the d -orbital energies due to the (a) bipyramidal and (b) octahedral crystal fields.

when the noncollinearity of Mn magnetic moments is considered. In particular, the calculations reveal that the polarization of h - $RMnO_3$ increases as r_{ion} decreases whereas that of o - $RMnO_3$ remains basically unaltered.

This paper is arranged as follows. A brief review of the relevant crystalline and magnetic structures is given in Sec. II. In Sec. III, we describe the technical aspects of our first-principles calculations. In Secs. IV A–IV C, we discuss the evolution of the energetic, atomic, and electronic properties of h - and o - $RMnO_3$ by substituting R with the late lanthanide elements. In Sec. IV D, we shall focus on the details of how the lattice effect, magnetic order, and the change in r_{ion} influence the ferroelectricity of the studied systems. Finally, the conclusion will be given in Sec. V.

II. CRYSTAL AND MAGNETIC STRUCTURE

Figure 1(a) illustrates the typical crystal structure for the hexagonal phase. It consists of nonconnected layers of MnO_5 trigonal bipyramids that are corner linked by planar oxygen $O1_p$ and $O2_p$. The apical oxygen $O1_a$ and $O2_a$ form two closely packed layers separated by a layer of displaced R ions. The $R1(R2)$ is located above the $O1_p$ ($O2_p$). The Mn ions are arranged in a two-dimensional triangular lattice, with successive layers relatively shifted from each other. The space group of h - $RMnO_3$ in the ferroelectric phase is $P6_3cm$. Compared to the high-temperature (HT) structure where all ions are constrained to planes parallel to the ab plane, the MnO_5 bipyramids are rotated about an axis through the Mn ion and parallel to the $O1_p$ - $O1_p$ interatomic bond accompanied by a tripling of the paraelectric unit cell to 30 atoms per unit cell. The resultant buckling moves the $O1_p$ up and the $O2_p$ down along the c axis and leads to vertical shifts of R ions away from the HT mirror plane.

As for the orthorhombic phase, it is easily seen in Fig. 1(b) that MnO_6 octahedra are of 3D connectivity, in sharp contrast to the bipyramid-layered structure in the hexagonal phase. The conventional unit cell (space group $Pbnm$) contains 4 f.u. The sizable mismatch of R -O and Mn-O bond lengths in the Goldschmidt tolerance factor $t \equiv (R-O)/[\sqrt{2}(Mn-O)] < 1$ results in a significant cooperative rotation of the octahedra, which increases with decreasing r_{ion} . This leads not only to the following lattice-parameter relation $b > a > c/\sqrt{2}$ but also to a bending of the Mn-O-Mn angle. The orbital overlap integral over the Mn-O-Mn bond-

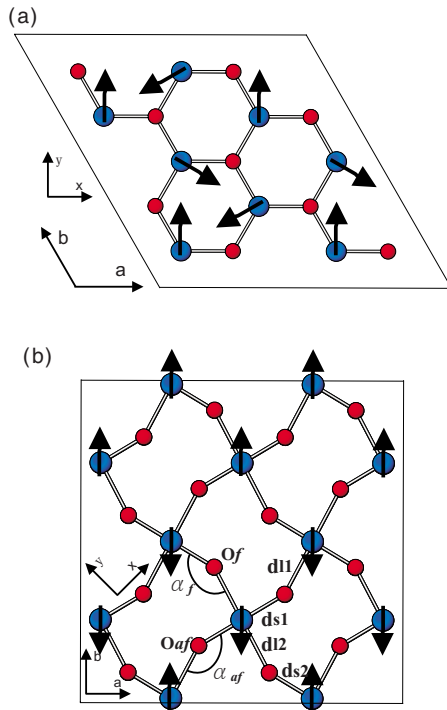


FIG. 3. (Color online) Mn magnetic structure of (a) hexagonal and (b) orthorhombic HoMnO_3 in the ab plane, antiferromagnetically coupled to the neighboring planes. Here, large balls denote Mn ions. Arrows indicate the direction of the local magnetic moment.

ing is therefore reduced. In addition, the Mn ion is JT active [Fig. 2(b)]. These phenomena have a profound influence on the physical properties, e.g., biasing the cooperative orbital and spin ordering^{4,26,27} and splitting the bond lengths at the octahedral site.

Figure 3 shows the Mn magnetic configurations in the basal plane for h - and o - HoMnO_3 . In the former case, the moments order in a NC 120° structure coupled antiferromagnetically to those in neighboring planes.^{16,17} As for the E -type phase in the orthorhombic structure, the FM zigzag chains are parallel to the a axis and have an AFM coupling with neighboring chains.

III. COMPUTATIONAL DETAILS

The present calculations were based on the generalized gradient approximation (GGA) (Ref. 39) to the exchange-correlation energy functional of the density-functional theory. The projector-augmented-wave potentials, as implemented in VASP,^{40,41} were employed with Mn $3d4s$, R $5p5d6s$, and O $2s2p$ electrons treated as valence electrons. The R $4f$ electrons in the potentials available so far were kept core frozen. We skipped the $R=\text{Yb}$ case due to the lack of corresponding compatible potential. The plane-wave basis set with an energy cutoff of 500 eV was used. The $5 \times 5 \times 3$ and $6 \times 3 \times 5$ Γ -centered grids were taken to sample the Brillouin zones of the hexagonal and orthorhombic supercells, respectively. We also performed the GGA+ U calculation⁴² with the commonly used values of $U=8.0$ eV

and $J=0.88$ eV,⁴³ which will be discussed later. The lattice parameters and atomic positions were relaxed until the total energy changed by less than 10^{-5} eV per conventional cell and the residual force was smaller than 0.01 eV/Å. The electronic contribution to the polarization of the compounds was obtained through the Berry phase using the modern theory of polarization.^{44–46} The contribution was calculated by integrating over 13 and 10 strings parallel to the c and a axis (the polarization direction) for the hexagonal and orthorhombic phases, with each string containing 3 and 5 \mathbf{k} points, respectively.

The NC calculations to simulate the triangularly frustrated magnetic moments were performed according to Ref. 47. The magnetic configuration of h - HoMnO_3 in Fig. 3(a) was adopted for the other three compounds. Under the triangular arrangement, our calculations showed no significant difference in the electronic structures from several different test orientations of the Mn moments. To our knowledge, the magnetic ordering of o - HoMnO_3 (Ref. 7) and o - LuMnO_3 (Ref. 48) at low temperatures (LTs) was confirmed to be the E type. Although that of o - ErMnO_3 was determined to be incommensurate with the propagation vector $q=(0, 0.433, 0)$,⁴⁹ we examined the approximate structure of $q \cong (0, 0.5, 0)$ for simplicity. Furthermore, based on Refs. 4, 8, and 26, the magnetic structure of o - TmMnO_3 was also assumed to be the E type in the present study.

IV. RESULTS AND DISCUSSION

A. Energetics

We first focus on the energetics of h - and o - RMnO_3 . In the former case, it has been reported³⁸ that the electronic property of h - YMnO_3 depends significantly on the Mn magnetic structure. Therefore, we calculate the total energies of h - RMnO_3 in the simple A type and the so-called frustrated A -type (frus_ A),³⁸ i.e., turning one of every three Mn same spins in the basal plane to the opposite direction. Additionally, the NC alignment of Fig. 3(a) is calculated for comparison. For the orthorhombic phase, besides the AFM E type, we also evaluate the AFM A -, C -, G -type, and FM cases. The GGA calculations are summarized in Table I, where the FM result is taken as a reference. It is clear that within the various spin configurations of interest, the total energies of the four h - RMnO_3 manganites are all lower than those for the corresponding orthorhombic phase, reflecting the preference of the late- R compounds for the hexagonal structure. The relative energetic favorability of the two structural phases is apparently dominated by the R -ion size and the hexagonal structure becomes more stable with smaller r_{ion} .⁵⁰ Moreover, the total-energy difference between these two structures substantially increases as R moves toward the end of the series. This implies the growing difficulty in converting h - RMnO_3 to the orthorhombic phase as r_{ion} decreases.

Now, we discuss the results of each phase separately. Take HoMnO_3 as one example. In the hexagonal phase, the frus_ A type leads to a significant lowering of 51 meV/f.u. in energy from the simple A type. With the realistic consideration of the triangular NC configuration, the total energy is further lowered by an amount of 6 meV/f.u. Similar trends

TABLE I. The calculated total energies (meV/f.u.) of $RMnO_3$ ($R=Ho, Er, Tm, Lu$) in various magnetic configurations: the A , frustrated A (frus_ A) types (Ref. 38) and NC ordering in the hexagonal phase, and the antiferromagnetic A , C , G , and E types and FM ordering in the orthorhombic phase. The notation E^* is explained in the text. The energies presented here are relative to the FM case.

Phase	Ho	Er	Tm	Lu
Hexagonal				
A	-100	-132	-170	-221
frus_ A	-151	-188	-232	-293
NC	-157	-194	-238	-300
Orthorhombic				
FM	0	0	0	0
A	-15	-16	-16	-14
C	-3	-5	-8	-10
G	-11	-14	-16	-17
E^*	-24	-25	-27	-28
E	-29	-30	-32	-33

are also observed in the other three manganites. Therefore, the magnetic order in h - $RMnO_3$ plays a crucial role in determining the energetics and the electronic structures, which will become clear shortly. In the orthorhombic phase, the E type indeed yields the lowest energy when compared to the cases of the A -, C -, G -, and FM types. These results indicate the importance of the AFM interactions through the Mn-O-O-Mn (Refs. 8 and 25) or the Mn-O-Mn (Ref. 4 and 26) path in predicting the correct ground state of o - $RMnO_3$. For further elaboration on the direction of the FM zigzag chains in the E -type phase, we also performed the calculation with the FM chains aligned along the b axis. The resultant total energy labeled E^* in Table I is found to be higher than that with the chains along the a axis. This is consistent with the fact that the commensurate magnetic modulation is along the b axis.⁷

B. Atomic structure

Since the total-energy calculations confirm that the magnetic ordering in the lowest-energy state is the NC 120° structure for the hexagonal phase and the E type for the orthorhombic phase, we shall focus on these two magnetic configurations in the rest of this paper.

Tables II and III list the fully optimized lattice parameters and the relevant bond lengths and bond angles for the hexagonal and orthorhombic phases, respectively. As can be concluded from these tables, the evaluated lattice constants are in good agreement with the experimental data⁴ (within 0.8%).

For the hexagonal phase at LT, the lattice parameters decrease with decreasing r_{ion} . This reflects the ionic character of R ions in h - $RMnO_3$. In fact, the $R-O_a$ bond lengths become smaller as r_{ion} is decreased and they remain basically unaltered from those of the HT phase. The decreasing lattice constant in the basal plane with the decreasing r_{ion} is associ-

TABLE II. The calculated lattice parameters and bond lengths (Å) of hexagonal $RMnO_3$ ($R=Ho, Er, Tm, Lu$) in low- and high-temperature phases.

	Ho	Er	Tm	Lu
Low temperature				
a	6.126	6.100	6.069	6.024
c	11.501	11.481	11.453	11.417
$R1-O1_a$	2.28	2.27	2.26	2.23
$R1-O2_a$	2.31	2.30	2.29	2.28
$R2-O1_a$	2.27	2.25	2.24	2.23
$R2-O2_a$	2.32	2.31	2.29	2.27
$R1-O1_p$	2.30	2.29	2.27	2.26
$R2-O2_p$	2.42	2.41	2.39	2.38
Mn- $O1_a$	1.89	1.89	1.89	1.89
Mn- $O2_a$	1.88	1.88	1.89	1.89
Mn- $O1_p$	2.06	2.06	2.05	2.03
Mn- $O2_p$	2.05	2.04	2.04	2.02
High temperature				
$a(\times\sqrt{3})$	6.187	6.154	6.118	6.060
c	11.342	11.347	11.354	11.363
$R-O_a$	2.27	2.26	2.25	2.23
$R-O_p$	2.84	2.84	2.84	2.84
Mn- O_a	1.88	1.88	1.88	1.89
Mn- O_p	2.06	2.05	2.04	2.02

ated with the shrinkage of the Mn- O_p bond lengths. However, the variation in r_{ion} has little effect on the Mn- O_a bond lengths, in agreement with the experimental observations.⁵¹ Table II shows that the occurrence of the structural phase transition from HT to LT is accompanied by shorter a and longer c lattice constants. Interestingly, the buckling of MnO_5 bipyramids gives no substantial change in the Mn-O bond lengths. Since there is little change in the $R-O_a$ bond lengths below T_C , the buckling leads to vertical shifts of R ions away from the HT mirror plane. As a result, in

TABLE III. The calculated lattice parameters (Å), in-plane Mn-O-Mn bond angles (°), and Mn-O bond lengths (Å) of orthorhombic $RMnO_3$ ($R=Ho, Er, Tm, Lu$). The bond angles and bond lengths refer to those in Fig. 3(b) and are explained in the text.

	Ho	Er	Tm	Lu
a	5.259	5.244	5.222	5.195
b	5.882	5.865	5.840	5.800
c	7.359	7.343	7.323	7.305
α_f	145.0	144.6	144.0	143.2
α_{af}	141.7	141.3	140.7	139.9
$d_{l,1}$	2.27	2.27	2.26	2.24
$d_{l,2}$	2.21	2.20	2.19	2.17
$d_{s,1}$	1.93	1.92	1.92	1.92
$d_{s,2}$	1.93	1.92	1.91	1.91

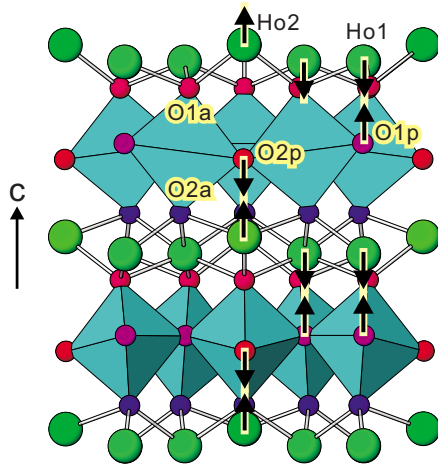


FIG. 4. (Color online) Schematic view of hexagonal HoMnO_3 in the ferroelectric state, with arrows indicating atomic displacements from the paraelectric structure.

HoMnO_3 , two of every three Ho-O_p bonds of 2.84 Å in the HT phase are reduced to 2.30 Å and the third to 2.42 Å. This asymmetry, as displayed in Fig. 4, will be shown later to be closely related to the existence of ferroelectricity in $h\text{-RMnO}_3$.

For the orthorhombic structure, Table III indicates that the lattice parameters evolve to smaller values as R approaches the end of the series, which is consistent with the experiment.⁴ It can be seen that the structure of $o\text{-RMnO}_3$ is highly distorted,³⁷ with the in-plane Mn-O-Mn angle being significantly smaller than the value of $\sim 155^\circ$ in LaMnO_3 .

Next, we discuss the magnetic effect on the atomic structure. The backbone of the E -type phase could be viewed as the sum of the A -type-like zigzag chains and the G -type-like interchains. To have a better understanding of the structural distortion caused by this magnetic order, we also investigate the optimized results of the paraelectric A and G types for comparison. For HoMnO_3 , it is found that the Mn-O-Mn bond angle α_f (143.8°) with parallel spins in the A type is larger than the α_{af} (142.4°) with antiparallel spins in the G type, a direct consequence of the Hund's coupling, and virtual electron hopping.²³ With the longest and shortest Mn-O bond length denoted as d_l and d_s , respectively, our calculations also show that the d_l (2.28 Å) of the G type is longer than that (2.21 Å) of the A type, although the d_s is almost the same (1.93 and 1.91 Å). However, when both types of spin alignments are present in the AFM- E phase, the atomic structure becomes more complicated as discussed below.

First, the α_f is flatter but the α_{af} is further distorted [refer to Fig. 3(b)]. Second, while the d_s still remains unchanged (1.92 Å), there exist two kinds of long Mn-O bonds: the FM $d_{l,1}$ of 2.27 Å and the AFM $d_{l,2}$ of 2.20 Å. Note that the $d_{l,1}$ is longer than the $d_{l,2}$, contrary to the expectations from the A - and G -type cases. Furthermore, a close examination of the optimized geometric structure reveals complicated atomic displacements with respect to the centrosymmetric A type.⁵² The calculations confirm that such an E -type configuration makes no significant displacement for all the ions along the c axis.²³ On the other hand, Fig. 5 indicates that along the b

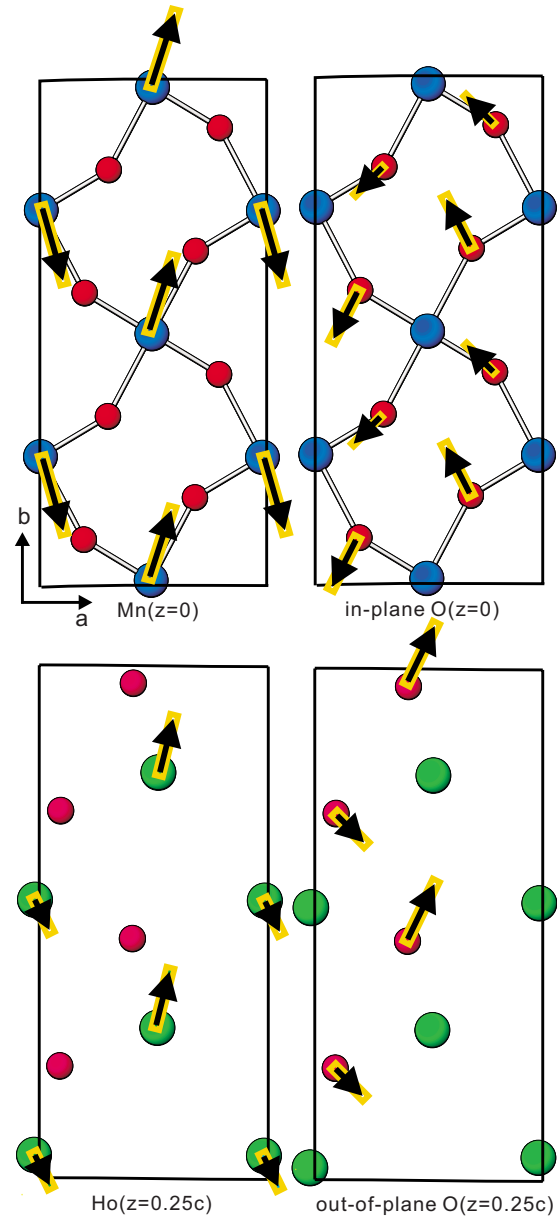


FIG. 5. (Color online) Atomic displacement of HoMnO_3 in the E -type phase with respect to the centrosymmetric A -type structure. The Mn spin moments are the same as those of the left part of Fig. 3(b).

direction Mn (in-plane O_{af}) ions shift by an amount of 0.03 Å (0.02 Å) compensating each other. The magnitude of the b component of O_f displacements is found to be only one third of that of O_{af} . However, the a component of the Mn (in-plane O) shift adds up to a net displacement of +0.01 Å (−0.01 Å). This result makes it clear that the α_f (α_{af}) becomes larger (smaller) in comparison with that of the A (G) type. It is worthy to point out that while the displacements of Ho (out-of-plane O) ions along the b direction are again equally opposite to each other, the a component shift is +0.005 Å (+0.01 Å). These will be shown in Sec. IV D to make an important contribution to the final ionic polarization.

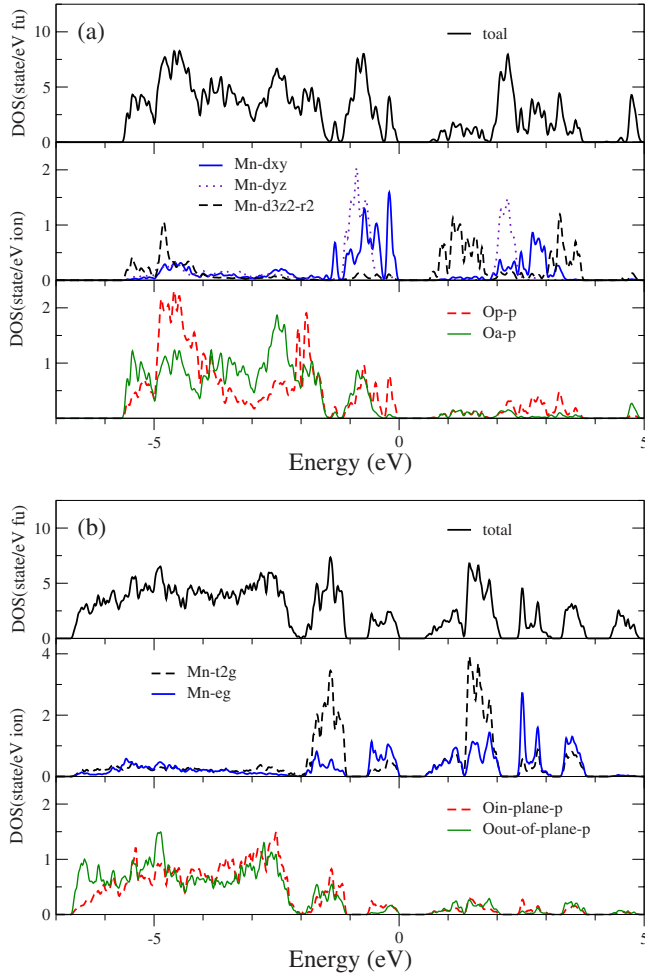


FIG. 6. (Color online) Orbital- and site-projected density of states (DOS) of (a) hexagonal and (b) orthorhombic HoMnO_3 . The abbreviation f.u. is for formula unit. Energy is relative to the valence-band maximum.

C. Electronic structures

Figure 6 depicts the orbital- and site-projected densities of states of HoMnO_3 , where the valence-band maximum (E_v) is set to zero. In the hexagonal phase, just below E_v is the Mn d_{xy} state hybridized with the $O_p p$ component. The lowest unoccupied band is dominated by the Mn $d(3z^2-r^2)$ and $O_a p$ states. The energy order of Mn d orbitals in Fig. 6(a) results from the bipyramidal crystal field. When compared with the experimental value⁵³ of ~ 1.7 eV, the electronic structure of the frus_A type opens up an energy gap (E_g) of 0.53 eV from a marginal value of 0.05 eV in the A type. The size of the gap is further increased to 0.75 eV in the more realistic NC treatment. We found that the frus_A type pushes the unoccupied Mn $d(3z^2-r^2)$ state up to the higher-energy region. In the NC case, while no significant difference was found between the main valence electronic structure and that of the frus_A type, the lowest unoccupied states are pushed further up. The prominent increase of E_g from its near gaplessness³⁵ in the A type implies the crucial role of the proper magnetic ordering in determining the electronic structure. It is interesting to note that the E_g of all the four com-

pounds studied here is about the same (the change ≤ 0.01 eV) and similar to that of $h\text{-YMnO}_3$.

In comparison with the hexagonal case, Fig. 6(b) clearly demonstrates that the major valence-state region of $o\text{-HoMnO}_3$ extends to the lower-energy region. This could be ascribed to the octahedron 3D network of the orthorhombic structure. As expected, there exists a splitting of 0.49 eV between the valence t_{2g} and e_g states owing to the octahedral crystal-field effect. The JT distortion and the tilting of the octahedra result in further splitting of e_g states and opening a gap of 0.54 eV. Nevertheless, unlike the hexagonal case, the E_g of $o\text{-RMnO}_3$ decreases slightly to 0.50 eV for the end compound LuMnO_3 . Note that, even without including the on-site Coulomb correlation U , the GGA scheme with the appropriate magnetic ordering already makes both hexagonal and orthorhombic phases insulating, an *a priori* property to exhibit ferroelectricity.

D. Ferroelectricity

Now, we turn to discuss the ferroelectricity developed in $h\text{-}$ and $o\text{-RMnO}_3$ manganites.

1. Hexagonal phase

As mentioned before, the $R\text{-O}_a$ bond lengths remain essentially unchanged despite the tilting of MnO_5 bipyramids. The R ions are forced to move vertically away from the HT mirror plane. Furthermore, the displacements of the $R1$ and $R2$ are considerably asymmetric. For example, Fig. 4 demonstrates that there are two kinds of $R\text{-O}_p\text{-R}$ vertical chains: $\text{Ho1-O1}_p\text{-Ho1}$ and $\text{Ho2-O2}_p\text{-Ho2}$. The segments Ho1-O1_p of 2.30 Å and the neighboring $\text{O1}_p\text{-Ho1}$ of 3.45 (11.50/2–2.30) Å are alternatively connected along the former chain, forming a “local” dipole moment. In the $\text{Ho2-O2}_p\text{-Ho2}$ chain, the successive atomic distances are 3.33 and 2.42 Å. This also gives rise to a dipole moment, yet with both size and direction being different from those of the $\text{Ho1-O1}_p\text{-Ho1}$ chain. Consequently, a net polarization could be established along the c axis. Although the individual local moments are relatively significant, those from every two $\text{Ho1-O1}_p\text{-Ho1}$ chains are partially canceled by the antiparallel moment due to one $\text{Ho2-O2}_p\text{-Ho2}$ chain, yielding a small resultant polarization. The total polarization of $h\text{-HoMnO}_3$ was found to be $8.0 \mu\text{C}/\text{cm}^2$, comparable to the experimental value⁵⁴ of $5.6 \mu\text{C}/\text{cm}^2$. This cancellation explains in part why the polarizations of $h\text{-RMnO}_3$ manganites are smaller than those of conventional perovskite ferroics [$\sim 25 \mu\text{C}/\text{cm}^2$ in BaTiO_3 and $\sim 75 \mu\text{C}/\text{cm}^2$ in PbTiO_3 (Ref. 55)]. Interestingly, Table IV shows a discernible trend that the polarization tends to be larger as r_{ion} decreases. According to Ref. 51, the difference between the two atomic distances in the $R\text{-O}_p\text{-R}$ segment is observed to increase with decreasing r_{ion} . From the simple argument described above, we indeed found that this difference increases as R approaches the end of the series, leading to an increase of the net dipole moment.⁵¹

Through group-theory analysis, it has been shown^{13,34} that the atomic displacements of $h\text{-RMnO}_3$ from the HT to LT phase could be decomposed into two main modes. One is the

TABLE IV. The calculated polarizations ($\mu\text{C}/\text{cm}^2$) of hexagonal and orthorhombic RMnO_3 ($R=\text{Ho, Er, Tm, Lu}$). The notations are explained in the text.

	Ho	Er	Tm	Lu
Hexagonal				
MM	2.6	2.7	2.7	2.8
RR	5.7	5.8	5.9	6.0
total	8.0	8.1	8.3	8.5
Orthorhombic				
P_{ion}	0.7	0.8	0.7	0.7
P_{ele}	5.0	5.0	5.0	5.2
P_{tot}	5.7	5.8	5.7	5.9
P'_{ele}	3.5	3.5	3.6	3.8
$P_{\text{ion,GGA+}U}$	0.2	0.2	0.2	0.2
$P_{\text{ele,GGA+}U}$	1.4	1.4	1.4	1.4
$P_{\text{tot,GGA+}U}$	1.6	1.6	1.6	1.6

so-called K_3 mode, which changes the symmetry but cannot create a macroscopic ferroelectric moment. Namely, the tilting of MnO_5 bipyramids causes a tripling of the paraelectric unit cell and by symmetry does not lead to an overall polarization. The other is the Γ_1 mode, which does not change the space-group symmetry but introduces the ferroelectricity. The latter mode is the component that involves the asymmetric displacements of R ions. To give a physical picture of how these two modes affect the ferroelectricity, we perform the polarization calculation by considering the following two structures: one with the atomic positions of R ions in the HT phase and those of MnO_5 polyhedra in the LT phase (MM) to mimic the K_3 mode and the other structure (RR) with the atomic positions of R ions and of MnO_5 polyhedra in the LT and HT phases, respectively, for the Γ_1 mode. From Table IV, it is clear that the resultant polarization of the MM structure is only about one third of the final polarization. A significant part of the final polarization comes from the RR structure, reflecting the important role of the asymmetry between $R\text{-O}_p$ and $\text{O}_p\text{-}R$ atomic distances in the ferroelectricity of $h\text{-RMnO}_3$.

At this stage, we attempt to probe the magnetic effect on the polarization of HoMnO_3 by comparing it with the non-magnetic calculations. However, the GGA electronic structures of the LT phase without magnetism are found to be metallic, with the lattice parameters and atomic positions being either fully relaxed or fixed as those obtained by the NC calculations. Therefore, we resort to the GGA+ U scheme in this issue. In the presence of NC magnetism, the GGA+ U polarization is not significantly different from the GGA. When the magnetism is turned off, the resultant polarization is found to be $17.9 \mu\text{C}/\text{cm}^2$, almost twice the value of $8.1 \mu\text{C}/\text{cm}^2$ obtained with inclusion of the NC ordering. The GGA+ U scheme without magnetism worsens the c -lattice parameter from 11.53 to 11.83 Å compared to the experimental value⁴ of 11.41 Å. In addition, the partial cancellation of the local moments between two $\text{Ho1-O1}_p\text{-Ho1}$ chains and one $\text{Ho2-O2}_p\text{-Ho2}$ chain becomes smaller, giving

rise to a larger net polarization. We concluded that the magnetism in $h\text{-RMnO}_3$ indirectly affects the final polarization through the sizable change in the atomic structure. Unfortunately, we cannot directly evaluate the contribution due to magnetism to the total polarization by performing the non-magnetic calculation with the atomic structure obtained by the GGA+ U scheme with the NC configuration since such a situation resumes its metallic behavior.

2. Orthorhombic phase

To demonstrate the spontaneous polarization in the E -type phase, we start with the Mn-O-Mn zigzag chain along the b axis with the A -type ordering. In this situation, all Mn-O-Mn segments are equivalent. Next, we replace the magnetic ordering by the E type, which is “up-up-down-down.” In order to optimize the exchange interactions in the FM and AFM segments, the zigzag chain will distort by transverse shifts of O anions to modulate the Mn-O-Mn angles and, consequently, modify exchange constants. According to the Goodenough-Kanamori-Anderson rules, the strength change in the FM and AFM exchanges will be opposite.⁵⁶ This requires the O to shift in the same direction, which breaks spatial inversion symmetry and results in a net polarization perpendicular to the chain.

In practical calculations, we choose the centrosymmetric and insulating A -type structure as the reference structure. Let us consider the HoMnO_3 case again. Table IV shows that the total polarization P_{tot} from the fully relaxed structure is $5.7 \mu\text{C}/\text{cm}^2$, which is about the same as the earlier works.^{23,37} The electronic contribution P_{ele} to this value is found to be $5.0 \mu\text{C}/\text{cm}^2$. It is noted that a non-negligible amount of $0.7 \mu\text{C}/\text{cm}^2$ due to the ionic dipole moment P_{ion} is also obtained. As mentioned in Sec. IV B, the E -type ordering leads to the off-center movements shown in Fig. 5. The dipole moment from the displacements of Mn and in-plane O is computed to be $-2.1 \mu\text{C}/\text{cm}^2$. However, the opposite shifts of Ho and out-of-plane O along the a axis together reverse the direction of the dipole moment, yielding a final ionic polarization of $0.7 \mu\text{C}/\text{cm}^2$ pointing in the positive a axis.

To elucidate the purely electronic effect owing to the E -type configuration, we evaluate the polarization using the optimized atomic positions of the A -type structure. Because of the structural centrosymmetry, there is clearly no ionic contribution. However, as seen from Table IV, the calculated electronic part (denoted as P'_{ele}) is $3.5 \mu\text{C}/\text{cm}^2$. This relatively large contribution comes mainly from the asymmetric electron distribution by the E -type ordering. An analysis of the residual forces on the ions shows that the b component of the forces on Mn and O_{af} is as large as $\sim 0.2 \text{ eV}/\text{Å}$ in magnitude. Particularly, for each ion species the residual forces along the a direction have the same sign and result in the net shifts in Fig. 5. Thus, under the E -type configuration, the electron wave function itself has lower symmetry than the lattice and creates ferroelectricity. This electronic asymmetry will further couple to the lattice and lead to lattice distortion. Therefore, when keeping the atoms fixed at the centrosymmetric positions, the E -type ordering will generate a purely electronic polarization and will apply forces on the atoms.

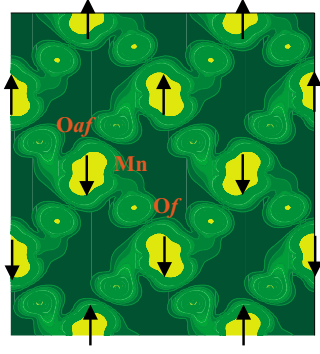


FIG. 7. (Color online) The MnO_2 plane charge-density contour of the E -type HoMnO_3 in the energy range $[-0.7:0]\text{eV}$ (valence-band maximum set as zero of the energy). Arrows denote the Mn spin moments.

These forces cause atomic displacements that will further influence the wave function. Such a specular ordering itself is the driving force of ferroelectricity in the orthorhombic phase, as opposed to the hexagonal case where the polarization is due primarily to the geometrical asymmetry of the atomic structure.

In Fig. 7, we plot the charge density of the occupied Mn e_g and O p states in the energy range between $E_v - 0.7\text{ eV}$ and E_v . In addition to the staggered ordering of the relevant e_g orbitals, this figure clearly demonstrates that there exists a strong asymmetry in the charge distribution between the Mn- O_f and Mn- O_{af} bonds. Therefore, the asymmetric electron distribution comes from a delicate combination of the JT effect and the symmetry-breaking E -type magnetic ordering.²³

However, the GGA polarization is much higher than the experimental value of $P < 2n\text{C}/\text{cm}^2$ measured in bulk polycrystalline HoMnO_3 samples.⁹ This substantial discrepancy is also observed in the cases of TbMn_2O_5 and HoMn_2O_5 .⁵⁷⁻⁵⁹ Although the polarization measured in polycrystalline samples tends to be underestimated and the role of R $4f$ electrons might need to be taken into account^{9,24} in theoretical investigation, very recent works^{59,60} have reported that for TbMn_2O_5 and HoMn_2O_5 , the ionic and electronic contributions obtained within the GGA+ U scheme are opposite in sign and almost cancel each other out, yielding a predicted total polarization in excellent agreement with the experiment. We are motivated by this aspect to test whether or not the inclusion of electron-electron correlation will drive a similar decimation of the resultant polarization of HoMnO_3 . As compared to the GGA results, the GGA+ U calculations show that both ionic $P_{\text{ion,GGA+}U}$ and electronic $P_{\text{ele,GGA+}U}$ contributions are reduced from 0.7 and 5.0 $\mu\text{C}/\text{cm}^2$ to 0.2 and 1.4 $\mu\text{C}/\text{cm}^2$, respectively. The suppression of the off centering in the atomic structure is expected since adding U makes the wave functions more localized and the virtual electrons hopping less favorable, rendering the electronic system more “rigid” and less susceptible to perturbation. However, even with U set as large as 8.0 eV, the remarkable sign change of HoMn_2O_5 by the GGA+ U cannot be obtained here for HoMnO_3 . One possibility is the lack of the existence of charge ordering in HoMnO_3 , which was used to argue for a near cancellation of the ionic and electronic con-

tributions and effectively reduces the polarization of HoMn_2O_5 .⁵⁹ Further theoretical and experimental works are needed to clarify this discrepancy for HoMnO_3 .

Finally, unlike the hexagonal case, Table IV shows that there is no significant change in the calculated polarizations as r_{ion} varies. This also reflects that the ferroelectricity in the orthorhombic phase is mainly due to the magnetism rather than the lattice structure, which is sensitive to the r_{ion} . Although we only discuss the origin of ferroelectricity in the two structural phases of HoMnO_3 , similar conclusions can be drawn for the other three compounds considered in the present study.

V. CONCLUSIONS

In conclusion, we have performed a systematic study of the energetic, atomic, electronic, and ferroelectric properties of RMnO_3 manganites ($R=\text{Ho, Er, Tm, and Lu}$) in both hexagonal and orthorhombic phases using first-principles calculations. We investigated the influence of the lattice, magnetic order, and the r_{ion} change in the ferroelectricity of these systems. In addition to the energetic preference for the hexagonal phase, it was found that the total-energy difference between the two crystal structures increases as r_{ion} decreases, reflecting the growing difficulty in converting the hexagonal phase to the orthorhombic one. As compared to the case of the previously considered frus_A type,³⁸ the size of the band gap for the hexagonal phase is improved when the 120° Mn magnetic configuration is taken into account. We analyzed the ferroelectricity through the evolution of the atomic structure. The calculations indicate that the polarization of $h\text{-RMnO}_3$ increases as r_{ion} decreases, while that of $o\text{-RMnO}_3$ remains basically unaltered.

Our results show that the driving force of ferroelectricity in $h\text{-RMnO}_3$ is the off centering of R ions along the c axis from the HT mirror plane. The role of magnetism in the hexagonal phase was found to stabilize the crystalline structure and indirectly influence the polarization. On the other hand, the underlying E -type magnetic ordering itself in the orthorhombic phase already breaks the inversion symmetry and is the main origin of the ferroelectricity observed. We found that a major portion of the polarization comes from the quantum-mechanical effect of the polarized electron orbitals, with a relatively smaller contribution arising from the atomic displacements. However, even with inclusion of the strong Coulomb correlation U , the large discrepancy between theory and experiment for the ferroelectricity of $o\text{-RMnO}_3$ still persists.

ACKNOWLEDGMENTS

The author is indebted to C. Cheng for enlightening discussions and critical reading of the manuscript. He also thanks T. C. Han and S. W. Cheong for useful discussions of experiments. Computer resources provided by the National Center for High-performance Computing are gratefully acknowledged. This work was supported by the National Science Council of Taiwan and National Center for Theoretical Sciences of Taiwan.

*cyren@nkn.edu.tw

- ¹ *Colossal Magnetoresistance, Charge Ordering, and Related properties of Manganese Oxides*, edited by C. N. R. Rao and B. Raveau (World Scientific, Singapore, 1998).
- ² T. Kimura, T. Goto, H. Shintani, K. Ishizaka, T. Arima, and Y. Tokura, *Nature* (London) **426**, 55 (2003).
- ³ T. Goto, T. Kimura, G. Lawes, A. P. Ramirez, and Y. Tokura, *Phys. Rev. Lett.* **92**, 257201 (2004).
- ⁴ J.-S. Zhou, J. B. Goodenough, J. M. Gallardo-Amores, E. Moran, M. A. Alario-Franco, and R. Caudillo, *Phys. Rev. B* **74**, 014422 (2006).
- ⁵ H. W. Brinks, H. Fjellvag, and A. Kjekshus, *J. Solid State Chem.* **129**, 334 (1997).
- ⁶ J. A. Alonso, M. J. Martinez-Lope, M. T. Casais, and M. T. Fernandez-Diaz, *Inorg. Chem.* **39**, 917 (2000).
- ⁷ A. Muñoz, M. T. Casáis, J. A. Alonso, M. J. Martinez-Lope, J. L. Martínez, and M. T. Fernández-Díaz, *Inorg. Chem.* **40**, 1020 (2001).
- ⁸ M. Tachibana, T. Shimoyama, H. Kawaji, T. Atake, and E. Takayama-Muromachi, *Phys. Rev. B* **75**, 144425 (2007).
- ⁹ B. Lorenz, Y. Q. Wang, and C. W. Chu, *Phys. Rev. B* **76**, 104405 (2007).
- ¹⁰ T. H. Lin, C. C. Hsieh, H. C. Shih, C. W. Luo, T. M. Uen, K. H. Wu, J. Y. Juang, J.-Y. Lin, C.-H. Hsu, and S. J. Liu, *Appl. Phys. Lett.* **92**, 132503 (2008).
- ¹¹ J. G. Lin, T. C. Han, C. T. Wu, M.-W. Chu, and C. H. Chen, *J. Cryst. Growth* **310**, 3878 (2008).
- ¹² For example, see S.-W. Cheong and M. Mostovoy, *Nature Mater.* **6**, 13 (2007); R. Ramesh and N. A. Spaldin, *ibid.* **6**, 21 (2007).
- ¹³ B. B. Van Aken, T. T. M. Palstra, A. Filippetti, and N. A. Spaldin, *Nature Mater.* **3**, 164 (2004).
- ¹⁴ E. F. Bertaut and M. Mercier, *Phys. Lett.* **5**, 27 (1963).
- ¹⁵ A. Muñoz, J. A. Alonso, M. J. Martinez-Lope, M. T. Casáis, J. L. Martínez, and M. T. Fernández-Díaz, *Phys. Rev. B* **62**, 9498 (2000).
- ¹⁶ T. Lottermoser, T. Lonkai, U. Amann, D. Hohlwein, J. Ihringer, and M. Fiebig, *Nature* (London) **430**, 541 (2004).
- ¹⁷ O. P. Vajk, M. Kenzelmann, J. W. Lynn, S. B. Kim, and S. W. Cheong, *Phys. Rev. Lett.* **94**, 087601 (2005).
- ¹⁸ G. A. Smolenskii and I. E. Chupis, *Sov. Phys. Usp.* **25**, 475 (1982) and references therein.
- ¹⁹ C. dela Cruz, F. Yen, B. Lorenz, Y. Q. Wang, Y. Y. Sun, M. M. Gospodinov and C. W. Chu, *Phys. Rev. B* **71**, 060407(R) (2005).
- ²⁰ T. Hotta, M. Moraghebi, A. Feiguin, A. Moreo, S. Yunoki, and E. Dagotto, *Phys. Rev. Lett.* **90**, 247203 (2003).
- ²¹ J. Salafranca and L. Brey, *Phys. Rev. B* **73**, 024422 (2006).
- ²² I. A. Sergienko, C. Sen, and E. Dagotto, *Phys. Rev. Lett.* **97**, 227204 (2006).
- ²³ S. Picozzi, K. Yamauchi, B. Sanyal, I. A. Sergienko, and E. Dagotto, *Phys. Rev. Lett.* **99**, 227201 (2007).
- ²⁴ B. Lorenz, Y. Q. Wang, Y. Y. Sun, and C. W. Chu, *Phys. Rev. B* **70**, 212412 (2004).
- ²⁵ T. Kimura, S. Ishihara, H. Shintani, T. Arima, K. T. Takahashi, K. Ishizaka, and Y. Tokura, *Phys. Rev. B* **68**, 060403(R) (2003).
- ²⁶ J.-S. Zhou and J. B. Goodenough, *Phys. Rev. Lett.* **96**, 247202 (2006).
- ²⁷ J.-S. Zhou and J. B. Goodenough, *Phys. Rev. B* **77**, 132104 (2008).
- ²⁸ H. Katsura, N. Nagaosa, and A. V. Balatsky, *Phys. Rev. Lett.* **95**, 057205 (2005).
- ²⁹ C. Jia, S. Onoda, N. Nagaosa, and J. H. Han, *Phys. Rev. B* **74**, 224444 (2006).
- ³⁰ I. A. Sergienko and E. Dagotto, *Phys. Rev. B* **73**, 094434 (2006).
- ³¹ C. D. Hu, *Phys. Rev. B* **77**, 174418 (2008).
- ³² A. Malashevich and D. Vanderbilt, *Phys. Rev. Lett.* **101**, 037210 (2008).
- ³³ H.-J. Xiang, S.-H. Wei, M.-H. Whangbo, and J. L. F. Da Silva, *Phys. Rev. Lett.* **101**, 037209 (2008).
- ³⁴ C. J. Fennie and K. M. Rabe, *Phys. Rev. B* **72**, 100103(R) (2005).
- ³⁵ A. Filippetti and N. A. Hill, *Phys. Rev. B* **65**, 195120 (2002).
- ³⁶ S. Picozzi, K. Yamauchi, G. Bihlmayer, and S. Blügel, *Phys. Rev. B* **74**, 094402 (2006).
- ³⁷ K. Yamauchi, F. Freimuth, S. Blügel, and S. Picozzi, *Phys. Rev. B* **78**, 014403 (2008).
- ³⁸ J. E. Medvedeva, V. I. Anisimov, M. A. Korotin, O. N. Mryasov, and A. J. Freeman, *J. Phys.: Condens. Matter* **12**, 4947 (2000).
- ³⁹ J. P. Perdew, K. Burke, and M. Ernzerhof, *Phys. Rev. Lett.* **77**, 3865 (1996).
- ⁴⁰ G. Kresse and D. Joubert, *Phys. Rev. B* **59**, 1758 (1999).
- ⁴¹ G. Kresse and J. Furthmüller, *Comput. Mater. Sci.* **6**, 15 (1996).
- ⁴² A. I. Liechtenstein, V. I. Anisimov, and J. Zaanen, *Phys. Rev. B* **52**, R5467 (1995).
- ⁴³ I. V. Solovyev, P. H. Dederichs, and V. I. Anisimov, *Phys. Rev. B* **50**, 16861 (1994).
- ⁴⁴ R. D. King-Smith and D. Vanderbilt, *Phys. Rev. B* **47**, 1651 (1993).
- ⁴⁵ D. Vanderbilt and R. D. King-Smith, *Phys. Rev. B* **48**, 4442 (1993).
- ⁴⁶ R. Resta, *Rev. Mod. Phys.* **66**, 899 (1994).
- ⁴⁷ D. Hobbs, G. Kresse, and J. Hafner, *Phys. Rev. B* **62**, 11556 (2000).
- ⁴⁸ H. Okamoto, N. Imamura, B. C. Hauback, M. Karppinen, H. Yamauchi, and H. Fjellvåg, *Solid State Commun.* **146**, 152 (2008).
- ⁴⁹ F. Ye, B. Lorenz, Q. Huang, Y. Q. Wang, Y. Y. Sun, C. W. Chu, J. A. Fernandez-Baca, Pengcheng Dai, and H. A. Mook, *Phys. Rev. B* **76**, 060402(R) (2007).
- ⁵⁰ Our calculations indeed show that the orthorhombic phase is energetically more stable than the hexagonal one for the $R = \text{La-Tb}$ cases.
- ⁵¹ B. B. Van Aken and T. T. M. Palstra, *Phys. Rev. B* **69**, 134113 (2004).
- ⁵² It is found that the fully relaxed FM-type structure is half metallic rather than insulating. For the later discussion of polarization, we choose the A-type structure as a reference.
- ⁵³ W. S. Choi, D. G. Kim, Sung Seok A. Seo, S. J. Moon, D. Lee, J. H. Lee, H. S. Lee, D. Y. Cho, Y. S. Lee, P. Murugavel, J. Yu, and T. W. Noh, *Phys. Rev. B* **77**, 045137 (2008).
- ⁵⁴ P. Coeuré, F. Guinet, J. C. Peuzin, G. Buisson, and E. F. Bertaut, in *Proceedings of International Meeting on Ferroelectricity*, edited by V. Dvorák (Institute of Physics of the Czechoslovak Academy of Sciences, Prague, 1996), p. 332–340.
- ⁵⁵ M. E. Lines and A. M. Glass, *Principles and Applications of Ferroelectrics and Related Materials* (Oxford University Press, Oxford, 2001).
- ⁵⁶ J. van den Brink and D. I. Khomskii, *J. Phys.: Condens. Matter* **20**, 434217 (2008).

- ⁵⁷C. Wang, G.-C. Guo, and L. He, Phys. Rev. Lett. **99**, 177202 (2007).
- ⁵⁸C. Wang, G.-C. Guo, and L. He, Phys. Rev. B **77**, 134113 (2008).

- ⁵⁹G. Giovannetti and J. van den Brink, Phys. Rev. Lett. **100**, 227603 (2008).
- ⁶⁰T.-R. Chang, H.-T. Jeng, C.-Y. Ren, and C.-S. Hsue (unpublished).